Nonmonotonic behavior as a function of nuclear charge of the *K*-shell Auger and radiative rates and fluorescence yields along the $1s2s^22p^3$ isoelectronic sequence

M. F. Hasoğlu,[1,*] D. Nikolić,[1] T. W. Gorczyca,[1] S. T. Manson,[2]
M. H. Chen,[3] and N. R. Badnell[4]
[1]*Department of Physics, Western Michigan University, Kalamazoo, Michigan 49008, USA*
[2]*Department of Physics and Astronomy, Georgia State University, Atlanta, Georgia 30303, USA*
[3]*Lawrence Livermore National Laboratory, Livermore, California 94550, USA*
[4]*Department of Physics, University of Strathclyde, Glasgow, G4 0NG, United Kingdom*
(Received 3 October 2007; revised manuscript received 12 June 2008; published 8 September 2008)

Calculations using multiconfiguration Breit-Pauli and multiconfiguration Dirac-Fock methodologies have revealed that the radiative and Auger rates, and the associated fluorescence yields, of the six electron $1s2s^22p^3$ *K*-shell vacancy isoelectronic sequence exhibit nonmonotonic behavior as a function of nuclear charge *Z*. This behavior is explained in terms of an accidental degeneracy, an avoided crossing of two nearly degenerate spin-orbit coupled levels. The results also demonstrate the importance of including both electron-electron correlation and spin-orbit effects even at low *Z*.

DOI: 10.1103/PhysRevA.78.032509 PACS number(s): 31.10.+z, 31.30.J−

I. INTRODUCTION

Unlike outer shells of atoms and ions, where the removal of an electron results in only limited relaxation and (generally) no further transitions, inner-shell ionization leads to very significant relaxation, i.e., inner-shell ionization is always followed by subsequent radiative and/or Auger transitions [1,2]. These rates and the associated fluorescence yields are indicators of the response (relaxation) of a system to the vacancy created by the excitation or ionization of an inner-shell electron. Specifically, the fluorescence yield is the measure of the fraction of these inner-shell vacancies that relax via emission of a photon (typically an x ray), as opposed to relaxation via nonradiative Auger decay. Denoting the radiative decay rate as A_r and the Auger decay rate as A_a, then the (*K* shell, for our purposes) fluorescence yield ω_K is defined as

$$\omega_K = \frac{A_r}{A_r + A_a}. \tag{1}$$

The fluorescence yields resulting from excitation or ionization of inner-shell electrons from neutral atoms have been the subject of numerous studies, experimental and theoretical [3,4]. For multicharged positive ions, there is effectively no experiment. But, there does exist a body of fairly recent theoretical work (see, for example, Refs. [5,6]), stimulated largely by the needs of x-ray astrophysics and plasma research, where a quantitative understanding of the creation and decay of inner-shell vacancies of atomic ions is of great importance. In particular, these data are used in various state-of-the-art astrophysical modeling codes [7–9]. Of significance here is the fact that much of the fluorescence yield data employed has resulted from hydrogenic interpolation and extrapolation techniques [10]. In this paper it is shown that such procedures could produce rather inaccurate results. Specifically, the present work explores the radiative and Auger decay rates of the $^3S_1$ and $^3P_1$ levels of the six-electron $1s2s^22p^3$ inner-shell-vacancy isoelectronic sequence, along with the associated fluorescence yields. Of particular interest is the nonmonotonic behavior of these rates, as a function of nuclear charge *Z* which translates to nonmonotonic behavior of the fluorescence yields, i.e., we find a radical departure from hydrogenic *Z* scaling of rates and the resulting fluorescence yields.

The hydrogenic *Z* scaling [11] of the decay rates, given by $A_r = A_{r1}Z^4$ and $A_a = A_{a1}Z^0$, is smooth. Therefore, the resulting fluorescence yield $\omega_K = (1+1/aZ^4)^{-1}$, with $a \equiv A_{r1}/A_{a1}$, generally exhibits monotonically increasing behavior $0 \leqslant \omega_K \underset{Z\to\infty}{\to} 1$ (see Fig. 1 for behavior using typical ratios $10^{-7} \leqslant a \leqslant 10^{-5}$). Of course, the nonhydrogenic screening leads to additional *Z*-dependent effects. But the smooth behavior depicted in Fig. 1 is generally found. This suggests that interpolation or extrapolation of computed to inferred

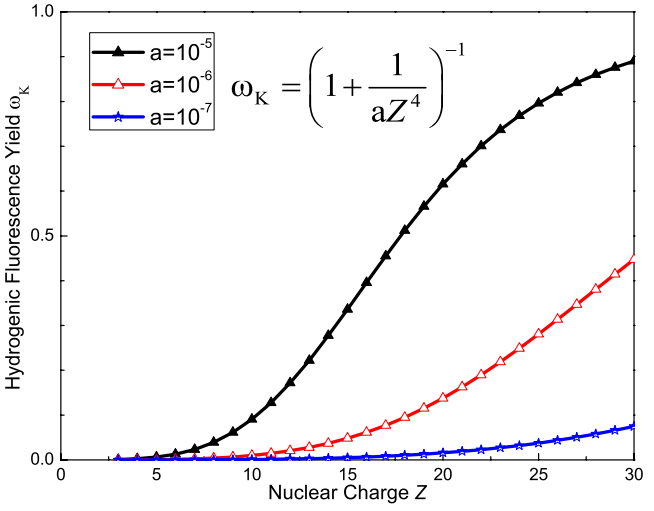

FIG. 1. (Color online) Hydrogenic behavior of the *K*-shell fluorescence yield as a function of nuclear charge *Z* for three typical values of the ratio *a* (defined in the text).

*fatih.hasoglu@wmich.edu

values [10] is possible. We show that such a procedure is grossly inaccurate in certain cases.

II. THEORETICAL METHODOLOGY

The atomic structure and collision code AUTOSTRUCTURE [12,13] is employed to calculate *ab initio* energy levels and rates A_r and A_a. These multiconfiguration Breit-Pauli (MCBP) calculations make use of nonrelativistic wave functions. Relativistic effects are included in the Hamiltonian, prior to diagonalization. Specifically, the entire Breit interaction in the Pauli form is included, viz., one- and two-body, fine and non-fine-structure operators [13–15]. All possible $2s^i2p^j$ configurations are included in the configuration interaction (CI) of both initial and final states of the system, the most important CI being the $2s^2 \rightarrow 2p^2$ intrashell correlation. Including this correlation goes beyond the single-particle model used to generate the most commonly used fluorescence and Auger yield data base [10]. These effects become increasingly important as the nuclear charge Z increases because certain decay pathways, forbidden in a single-particle nonrelativistic calculation, become significant with the inclusion of CI and relativistic effects. We investigated the inclusion of higher $n=2 \rightarrow 3$ correlation (all possible $2s^i2p^j3s^k3p^l3d^m$ configurations) and found that these additional configurations affect the computed radiative rates by less than 5%, so we chose to omit them. We note that a similar study on radiative and Auger rates of Fe^{17+}-Fe^{24+}, which included the carbonlike Fe^{20+} as we have for our present case, concluded that "It is found that CI from configurations with $n=3$ orbitals is of little importance and can be practically neglected" [16].

In addition, we have implemented a method within the AUTOSTRUCTURE atomic code [12] in which separate orbital basis sets are used to describe each individual configuration and, hence, the initial and final states. Thus, important relaxation effects—the difference in the atomic orbitals between the K-shell-vacancy and full-K-shell wave functions due to different $1s$ screening (one in the former, two in the latter)—are accounted for. The only approximation used in this approach is that the overlap integrals are all assumed to be unity or zero, as if the orbital basis were orthogonal. This is similar to the approach taken by Cowan [11]. Furthermore, the uncertainty introduced by this approximation can be assessed by determining and utilizing the overlap integrals which would otherwise be taken to be unity. The contribution from terms involving overlap integrals taken to be zero can be expected to be of similar magnitude. We have confirmed that this approximation holds quite well for the present case, introducing uncertainties of $\approx 5\%$ in the computed rates.

We have also used a multiconfiguration Dirac-Fock (MCDF) method [17]. As this approach is based on the full Dirac-Fock equation, including large and small component wavefunctions, it implicitly includes many relativistic effects on an *ab initio* basis. In addition to all of the relativistic corrections that are included perturbatively in the MCBP method, the MCDF method also accounts for the frequency-dependent generalized Breit interaction, and quantum electrodynamic (QED) corrections. For heavy elements, the MCBP approach using nonrelativistic wave functions will be inappropriate since not all relativistic effects can be treated perturbatively at high Z.

We have performed new MCDF calculations using an improved code [18] that has been augmented to treat the low-Z region better. In Ref. [17], the initial and final states are included in the same MCDF calculation. The procedure leads to some compromise in the energy levels and orbital wave functions that cause the greatest inaccuracies in the low-Z region. The new MCDF calculations are carried out using an extended-averaged level scheme [18,19] for the initial and final states separately including the same CI expansion from the $n=2$ complex as is used for the MCBP calculations (all possible $2s^i2p^j$ configurations are included in the CI of both initial and final states of the system). In this extended-averaged level scheme, the orbital wave functions are obtained by minimizing the statistical-weight-averaged energy of all the levels in the MCDF expansion. Since the initial and final states are treated separately, relaxation effects are included in this method in exactly the same manner as the MCBP method described above, including the approximation that the overlap integrals are taken to be either unity or zero. The transition energies and eigenvectors also include contributions from the generalized Breit interaction and QED corrections. For the lighter elements of astrophysical importance, $Z \leqslant 30$, we have found that these two approaches are usually in quite good agreement for fluorescence yield calculations [20–22] and dielectronic recombination of numerous ions (see, for example, Refs. [23–25]).

III. RESULTS AND DISCUSSION

To begin with, our MCBP and new MCDF results for A_r and A_a vs Z are given in Figs. 2 and 3. The same CI description—the entire $n=1,2$ complex for initial and final states—is used in both calculations. It is seen that both exhibit the same qualitative behavior. Furthermore, at higher Z, the MCBP and MCDF results for A_r and A_a differ by not more than about 5%. Since relativistic effects become increasingly important as Z is increased, this suggests strongly that the perturbative inclusion of relativistic effects in the MCBP approach works well for $Z \leqslant 30$. However, there are larger differences at lower Z which we attribute to differences in zero-order wave functions employed. A useful measure of the quality of multiconfiguration calculations of radiative rates can be obtained by comparing the results obtained from calculations in both "length" and "velocity" gauges [14]. The results are identical if exact wave functions are used. However, in practice, approximate wave functions are used and the difference is an indication of the accuracy of the calculations. A selection of MCBP and MCDF results is shown in Table I. For $Z=7$, it is seen that the MCBP length and velocity rates differ by up to about 10%, while for the MCDF case, differences of upwards of 70% are found. At the higher values of Z, the length-velocity agreement improves for both calculations: about 5% for MCBP and to within 10% for MCDF. Unfortunately, while this length-velocity agreement is a good indicator for calculations based on a Schrödinger equation similar to MCBP, it is less useful for

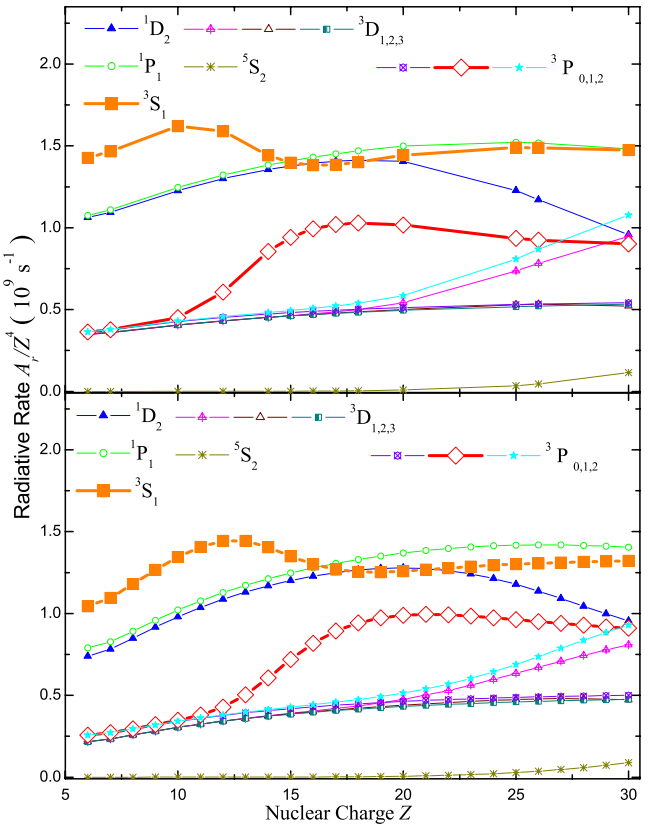

FIG. 2. (Color online) Calculated MCDF (top) and MCBP (bottom) radiative A_r rates for the ten K-shell vacancy levels $1s2s^22p^3(^{2S+1}L_J)$ of the C-like isoelectronic sequence. Note that A_r is scaled by $1/Z^4$ to factor out the strong Z^4 dependence.

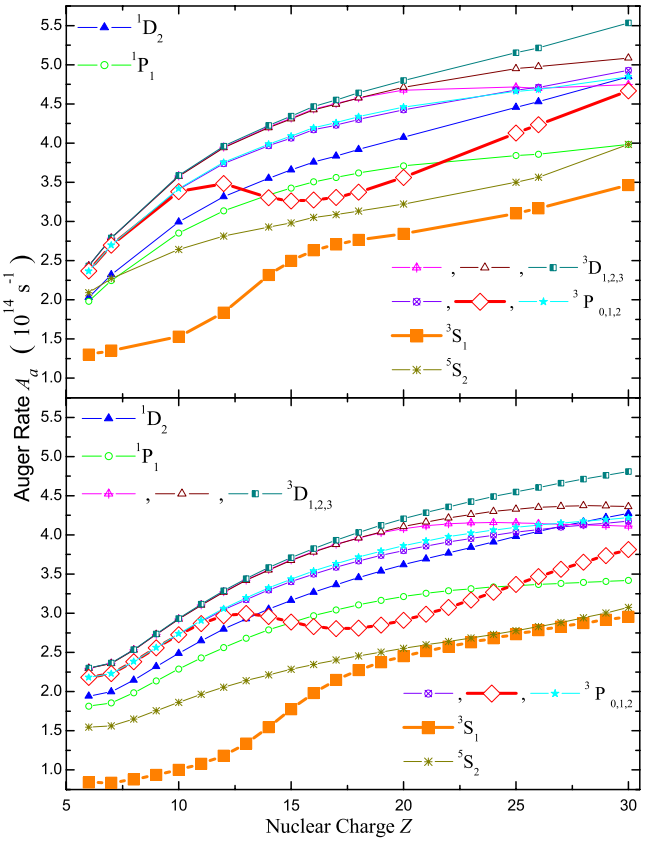

FIG. 3. (Color online) Calculated MCDF (top) and MCBP (bottom) Auger rates A_a for the ten K-shell vacancy levels $1s2s^22p^3(^{2S+1}L_J)$ of the C-like isoelectronic sequence.

calculations based on the Dirac equation, such as MCDF, where it is known that the velocity form is generally to be preferred [26] and that length-form convergence is slow. As a corroboration of these ideas, note that in almost every case shown in Table I, the MCDF-velocity result is in much better agreement with the MCBP results than the MCDF-length rates. In any case, based upon the comparison of length and velocity gauges, it appears that the MCBP results are reasonably accurate.

The total Auger and radiative rates (the latter Z scaled for clarity) are shown for all ten levels of the $1s2s^22p^3$ configuration in Figs. 2 and 3, respectively; all of these curves would appear as horizontal lines in the hydrogenic case. Eight of the ten levels show deviations from the constant hydrogenic prediction, but appear as simple smooth curves. On the other hand, two levels $1s2s^22p^3(^3P_1)$ and $1s2s^22p^3(^3S_1)$ exhibit nonmonotonic behavior in the region $Z\approx 15$. The nonmonotonic behavior of these two levels is also manifested in the resulting fluorescence yields, as seen in Fig. 4. However, the erratic behavior is somewhat less pronounced since it is a ratio of two rates. The other eight fluorescence yields, being ratios of smooth curves, are themselves seen to be smooth. Thus, the question facing us is: why do two of the levels of the $1s2s^22p^3$ K-shell-vacancy configuration exhibit erratic behavior along the isoelectronic sequence, but the other eight do not. Note that the phenomenology is exactly the same in both the MCBP and MCDF results, the small differences between them notwithstanding. The fact that we get precisely the same phenomenology using a MCPB methodology (based upon the Schrödinger equation) and MCDF (based on the Dirac equation) is convincing evidence that the nonmonotonic behavior is not a calculational artifact. In what follows, then, the situation is analyzed in the simpler MCBP framework.

To understand this phenomenology, we note first that the two levels exhibiting nonmonotonic behavior are both $J=1$. Since the $^3S_1$ and $^3P_1$ levels are not coupled within the nonrelativistic Hamiltonian, any interaction between them must be due to relativistic effects. The strongest relativistic effect for multicharged ions is the spin-orbit interaction. But, the spin-orbit coupling matrix element increases rapidly with increasing Z. This suggests that any effect arising from spin-orbit coupling between the levels should be largest at the highest Z, which is not what is seen. However, from a perturbation theory point of view, the full coupling coefficient is the coupling matrix element divided by the energy difference, thus suggesting the possibility of an accidental degeneracy of the nonrelativistic (LS) energies of the two levels in question in the $Z\approx 15$ region, i.e., an energy level crossing as a function of Z. In fact there is an accidental degeneracy which is similar to the well-known Von Neumann-Wigner [27,28] avoided crossings. This is the explanation for the observed phenomenon.

Specifically, we focus on three single-configuration (SC) $J=1$ levels $|^3S_1\rangle \leftrightarrow 1s2s^22p^3(^3S_1)$, $|^3P_1^a\rangle \leftrightarrow 1s2s^22p^3(^3P_1)$,

TABLE I. Comparison of radiative rates (s^{-1}) of selected levels of the $1s2s^22p^3$ isoelectronic sequence in length and velocity gauges for MCBP and MCDF calculations.

Z	Level	MCBP^L	MCBP^V	MCDF^L	MCDF^V
7	$^5S_2$	8.54×10^{6}	8.21×10^{6}	3.98×10^{7}	5.08×10^{7}
	$^3D_1$	5.62×10^{11}	5.87×10^{11}	8.61×10^{11}	5.05×10^{11}
	$^3D_2$	5.62×10^{11}	5.87×10^{11}	8.64×10^{11}	5.09×10^{11}
	$^3D_3$	5.62×10^{11}	5.87×10^{11}	8.68×10^{11}	5.13×10^{11}
	$^3S_1$	2.63×10^{12}	2.36×10^{12}	3.52×10^{12}	2.04×10^{12}
	$^3P_0$	6.53×10^{11}	6.06×10^{11}	9.04×10^{11}	5.28×10^{11}
	$^3P_1$	6.54×10^{11}	6.06×10^{11}	9.06×10^{11}	5.31×10^{11}
	$^3P_2$	6.53×10^{11}	6.06×10^{11}	9.08×10^{11}	5.33×10^{11}
	$^1D_2$	1.88×10^{12}	1.77×10^{12}	2.63×10^{12}	1.53×10^{12}
	$^1P_1$	1.99×10^{12}	1.79×10^{12}	2.66×10^{12}	1.55×10^{12}
12	$^5S_2$	3.75×10^{9}	3.68×10^{9}	5.99×10^{9}	5.26×10^{9}
	$^3D_1$	7.12×10^{12}	7.32×10^{12}	8.92×10^{12}	7.25×10^{12}
	$^3D_2$	7.10×10^{12}	7.31×10^{12}	8.93×10^{12}	7.27×10^{12}
	$^3D_3$	7.09×10^{12}	7.31×10^{12}	8.96×10^{12}	7.30×10^{12}
	$^3S_1$	2.99×10^{13}	2.83×10^{13}	3.30×10^{13}	2.66×10^{13}
	$^3P_0$	7.83×10^{12}	7.53×10^{12}	9.38×10^{12}	7.50×10^{12}
	$^3P_1$	8.88×10^{12}	8.51×10^{12}	1.26×10^{13}	1.01×10^{13}
	$^3P_2$	7.87×10^{12}	7.57×10^{12}	9.47×10^{12}	7.59×10^{12}
	$^1D_2$	2.25×10^{13}	2.19×10^{13}	2.70×10^{13}	2.18×10^{13}
	$^1P_1$	2.34×10^{13}	2.22×10^{13}	2.74×10^{13}	2.21×10^{13}
20	$^5S_2$	9.89×10^{11}	9.96×10^{11}	1.27×10^{12}	1.15×10^{12}
	$^3D_1$	7.61×10^{13}	7.79×10^{13}	8.67×10^{13}	7.82×10^{13}
	$^3D_2$	7.04×10^{13}	7.23×10^{13}	8.01×10^{13}	7.25×10^{13}
	$^3D_3$	6.91×10^{13}	7.15×10^{13}	7.93×10^{13}	7.20×10^{13}
	$^3S_1$	2.01×10^{14}	1.99×10^{14}	2.31×10^{14}	2.08×10^{14}
	$^3P_0$	7.40×10^{13}	7.33×10^{13}	8.21×10^{13}	7.33×10^{13}
	$^3P_1$	1.58×10^{14}	1.56×10^{14}	1.63×10^{14}	1.46×10^{14}
	$^3P_2$	8.23×10^{13}	8.22×10^{13}	9.36×10^{13}	8.40×10^{13}
	$^1D_2$	2.05×10^{14}	2.04×10^{14}	2.25×10^{14}	2.03×10^{14}
	$^1P_1$	2.19×10^{14}	2.16×10^{14}	2.40×10^{14}	2.16×10^{14}
25	$^5S_2$	1.09×10^{13}	1.11×10^{13}	1.38×10^{13}	1.27×10^{13}
	$^3D_1$	2.48×10^{14}	2.54×10^{14}	2.87×10^{14}	2.66×10^{14}
	$^3D_2$	1.85×10^{14}	1.92×10^{14}	2.07×10^{14}	1.92×10^{14}
	$^3D_3$	1.79×10^{14}	1.88×10^{14}	2.02×10^{14}	1.88×10^{14}
	$^3S_1$	5.09×10^{14}	5.12×10^{14}	5.82×10^{14}	5.39×10^{14}
	$^3P_0$	1.90×10^{14}	1.92×10^{14}	2.07×10^{14}	1.90×10^{14}
	$^3P_1$	3.76×10^{14}	3.78×10^{14}	3.66×10^{14}	3.38×10^{14}
	$^3P_2$	2.69×10^{14}	2.74×10^{14}	3.16×10^{14}	2.92×10^{14}
	$^1D_2$	4.60×10^{14}	4.68×10^{14}	4.80×10^{14}	4.45×10^{14}
	$^1P_1$	5.54×10^{14}	5.57×10^{14}	5.95×10^{14}	5.50×10^{14}
30	$^5S_2$	7.24×10^{13}	7.57×10^{13}	9.26×10^{13}	8.70×10^{13}
	$^3D_1$	6.55×10^{14}	6.80×10^{14}	7.68×10^{14}	7.23×10^{14}
	$^3D_2$	3.82×10^{14}	4.02×10^{14}	4.22×10^{14}	3.98×10^{14}
	$^3D_3$	3.85×10^{14}	4.09×10^{14}	4.32×10^{14}	4.08×10^{14}
	$^3S_1$	1.07×10^{15}	1.10×10^{15}	1.19×10^{15}	1.13×10^{15}
	$^3P_0$	4.06×10^{14}	4.17×10^{14}	4.39×10^{14}	4.10×10^{14}
	$^3P_1$	7.37×10^{14}	7.58×10^{14}	7.29×10^{14}	6.85×10^{14}
	$^3P_2$	7.52×10^{14}	7.81×10^{14}	8.72×10^{14}	8.22×10^{14}
	$^1D_2$	7.73×10^{14}	8.00×10^{14}	7.76×10^{14}	7.30×10^{14}
	$^1P_1$	1.14×10^{15}	1.17×10^{15}	1.20×10^{15}	1.13×10^{15}

and $|^3P_1^b\rangle \leftrightarrow 1s2p^5(^3P_1)$. At the SC level of approximation, $E(^3S_1) \sim E(^3P_1^a)$ and these energies are both much lower than $E(^3P_1^b)$. Our calculations show that the SC levels $|^3P_1^a\rangle$ and $|^3P_1^b\rangle$, which have the same LS quantum numbers and differ by only two electrons, are significantly mixed via CI. We denote the lower mixed as $|(^3P_1)\rangle$. Although mixed, it is composed primarily of the $1s2s^22p^3$ configuration. Specifically, it is a mixture $|(^3P_1)\rangle = c_a|^3P_1^a\rangle + c_b|^3P_1^b\rangle$. Since the SC energies of the two levels are well separated, a simple perturbative approach is valid. Defining $V_{\rm CI} = \langle ^3P_1^a|\Sigma_{j>i}\frac{1}{r_{ij}}|^3P_1^b\rangle$, $|c_b/c_a| \approx |V_{\rm CI}/(E_b - E_a)| \approx 0.1$ for all Z since the numerator and denominator both scale linearly as Z [11]. This CI has a most interesting effect upon the energy of the $1s2s^22p^3(^3P_1)$ level as seen in Fig. 5(a), which shows the energy separation (scaled by Z) of this level from the $^3S_1$ level. At the CI level approximation there is a level crossing around $Z=20$, but the crossing is absent at the SC level. It is thus evident that the inclusion of CI effects is crucial to the existence of the level crossing.

With the inclusion of relativistic effects into the calculation, there is a nonzero matrix element between the $^3P_1$ and

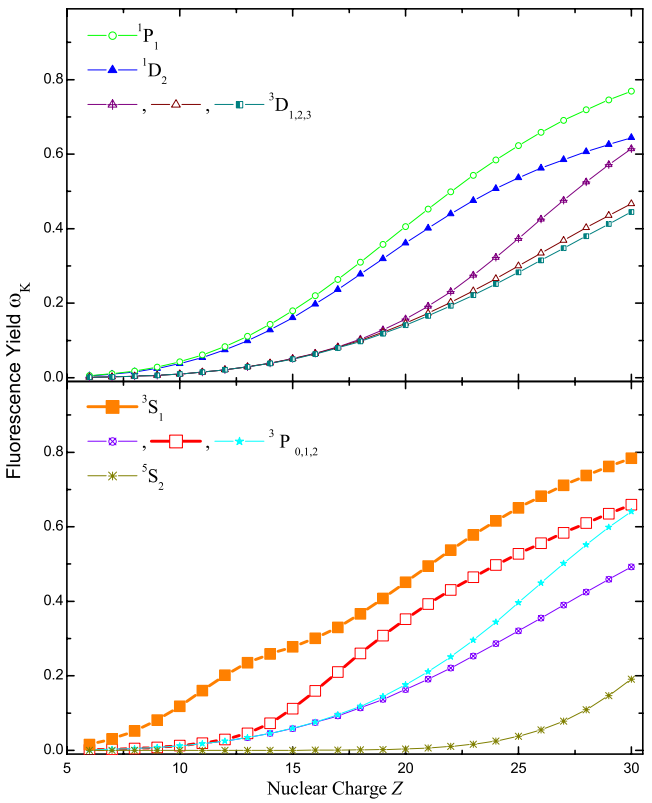

FIG. 4. (Color online) Calculated fluorescence yields ω_K for the K-shell vacancy C-like $1s2s^22p^3(^{2S+1}L_J)$ isoelectronic sequence.

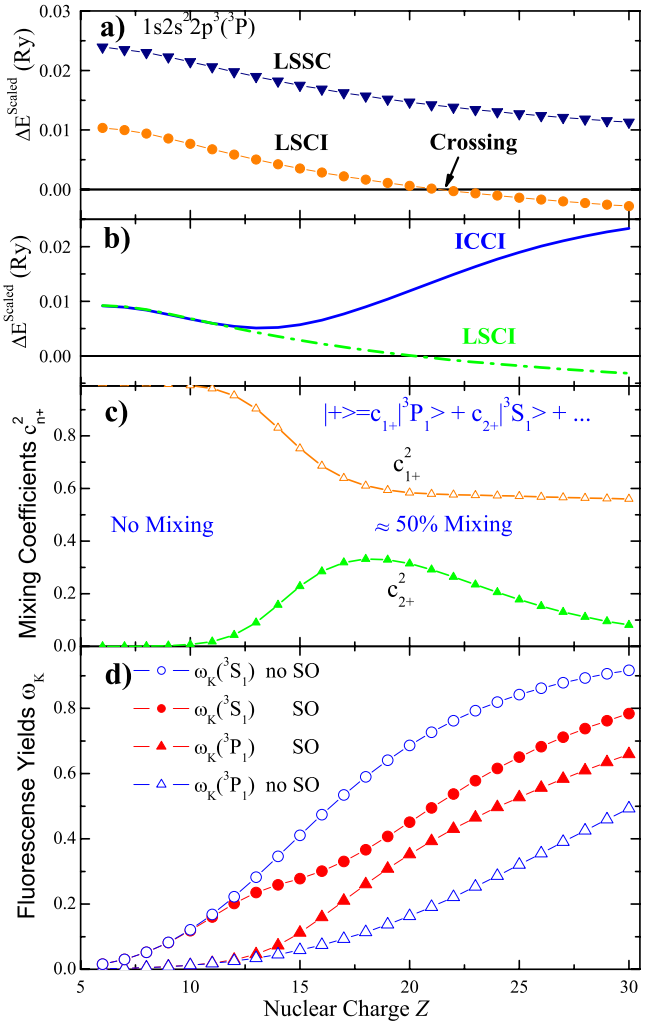

FIG. 5. (Color online) (a) $\Delta E^{\text{scaled}}=[E(^3P)-E(^3S)]/Z$ within the $1s2s^22p^3$ configuration using nonrelativistic single configuration (LSSC) and configuration interaction (LSCI) approximations. (b) ΔE^{scaled} within the $1s2s^22p^3$ configuration using nonrelativistic (LSCI) and relativistic configuration-interaction, in an intermediate coupling scheme (ICCI). (c) Mixing coefficients for the relativistically (spin-orbit) mixed $^3P_1$ and $^3S_1$ levels of the $1s2s^22p^3$ configuration. (d) Fluorescence yields excluding and including spin-orbit (SO) effects for the $1s2s^22p^3(^3P_1)$ and $1s2s^22p^3(^3S_1)$ levels. The nonmonotonic fluorescence yield behavior is seen to occur once there is appreciable spin-orbit mixing $c_{2+}^2 \lesssim c_{1+}^2$.

$^3S_1$ levels, principally through the spin-orbit interaction. This, of course, leads to an avoided crossing, as shown in Fig. 5(b); note the striking similarity with Fig. 10-2 of Ref. [11]. The energy splitting between the two levels is seen to be smallest in the region of $Z=15$, exactly the region where the nonmonotonic behavior in rates and fluorescence yields for the two levels was seen to occur. We emphasize that the inclusion of both CI and spin-orbit effects in the calculation is required to produce the avoided crossing, even qualitatively.

Quantitatively, to an excellent approximation, we have a two-level system [29], interacting through the (relatively weak) spin-orbit interaction. Writing the two spin-orbit-mixed levels as $|\pm\rangle=c_{1\pm}|^3S_1\rangle+c_{2\pm}|^3P_1\rangle$ leads us to the (nonperturbative) determinantal equation

$$\begin{pmatrix} E(^3S_1)-E & V_{\text{SO}} \\ V_{\text{SO}} & E(^3P_1)-E \end{pmatrix}\begin{pmatrix} c_{1\pm} \\ c_{2\pm} \end{pmatrix}=\begin{pmatrix} 0 \\ 0 \end{pmatrix}.$$

We solved this pair of equations and the results are shown in Fig. 5(c). It is evident that there is essentially no mixing of these two levels at low-Z and nearly 50-50 mixing around $Z=20$, i.e., $|c_{2\pm}/c_{1\pm}|^2 \approx 1/2$, the well-known result for near degeneracy. In other words, in this region the maximum mixing of $^3S_1$ and $^3P_1$ characters in each level occurs and, therefore, a "sharing" of radiative and Auger rates and, hence, a strong deviation from the otherwise-smooth behavior. The sum remains smooth, by unitarity, as can also be inferred from Figs. 2 and 3.

To emphasize the effect of this mixing via the spin-orbit interaction, the calculated fluorescence yields ω_K for the $^3S_1$ and $^3P_1$ levels are shown in Fig. 5(d), both with and without the inclusion of spin-orbit effects. Our results demonstrate that the results calculated without the spin-orbit interaction do not show the nonmonotonic behavior that is so pronounced in the full calculation [also shown in Fig. 5(d)]. Thus, it is spin-orbit mixing, in the region of the avoided crossing, that is responsible for the nonmonotonic behavior. The crucial comparison here is the relative magnitude of the (small) spin-orbit interaction matrix element between the two levels vs the electrostatic splitting between them. At this point, it is worthwhile to emphasize that both CI and relativistic effects are required not only to get the correct quantitative behavior, but even to get the correct qualitative behavior.

In that sense, the results presented herein detail a specific case of a general phenomenon. In fact another case of this general phenomenon, a small interaction having a significant effect owing to accidental degeneracies (level crossings) was found previously in connection with photoionization of Ne [30,31] where the spin-orbit interaction caused dramatic alteration of certain photoelectron angular distributions owing to accidental near degeneracies.

In addition, it is entirely possible that the nonmonotonic behavior of radiative and nonradiative rates, along with the associated fluorescence yields, occurs in other cases as well. A similar nonmonotonic behavior as a function of nuclear charge Z has been noted in effective collision strengths for the same F-like sequence [32] and, in fact, the cause of this behavior can be traced to a similar energy-crossing phenomenon, as we have noted in the present paper, giving rise to appreciable term mixing via the spin-orbit operator [compare Figs. 24 and 25 of Ref. [32] at $Z=31$ with the present Figs. 4(c) and 4(d) near $Z\approx 20$].

IV. CONCLUSION

In conclusion it has been demonstrated that higher-order CI, spin-orbit, and energy level crossing effects, all considered together, result in nonmonotonic behavior of the calculated radiative and Auger rates and fluorescence yields for the K-shell in the $1s2s^22p^3$ isoelectronic sequence. This behavior is understood within the framework of the Von

Neumann-Wigner [27] avoided crossings phenomena whereby an accidental degeneracy, or crossing, of the $1s2s^22p^3(^3P_1)$ and $1s2s^22p^3(^3S_1)$ nonrelativistic energies at $Z \approx 20$ results in significant spin-orbit mixing (nearly 50% of each). This in turn leads to radiative and Auger rates and, hence, fluorescence yields from levels of mixed character and nonmonotonic behavior as a function of Z in that locale. Thus, interpolation and extrapolation of rates and yields along an isoelectronic sequence is unsafe, in general, and explicit calculations for each member of a sequence are necessary so as to provide the necessary atomic data for astrophysical modeling.

ACKNOWLEDGMENTS

M.F.H, D.N., and T.W.G. were supported in part by NASA APRA Grant No. NNG0-4GB58G and NASA SHP SR&T Grant No. NNG05GD41G. S.T.M. was supported in part by NASA APRA Grant No. NAG5-12712 and NSF Grant No. PHY-0244394. The work of M.H.C. was performed under the auspices of U.S. Department of Energy by Lawrence Livermore National Laboratory under Contract No. DE-AC52-07NA27344. N.R.B. was supported in part by UK PPARC Grant No. PPA-G/S2003/00055.

[1] B. Crasemann, *Atomic Inner-Shell Processes* (Academic Press, New York, 1975).
[2] B. Crasemann, *Atomic Inner-Shell Physics* (Plenum Press, New York, 1985).
[3] J. H. Hubbell, P. N. Trehan, Nirmal Singh, B. Chand, D. Mehta, M. L. Garg, R. R. Garg, Surinder Singh, and S. Puri, J. Phys. Chem. Ref. Data **23**, 339 (1994).
[4] E. J. McGuire, Phys. Rev. **161**, 51 (1967); **185**, 1 (1969); Phys. Rev. A **2**, 273 (1970); **3**, 587 (1971); **5**, 1052 (1972).
[5] M. H. Chen and B. Crasemann, Phys. Rev. A **35**, 4579 (1987).
[6] J. Garcia, C. Mendoza, M. A. Bautista, T. W. Gorczyca, T. R. Kallman, and P. Palmeri, Astrophys. J., Suppl. Ser. **158**, 68 (2005).
[7] G. J. Ferland, K. T. Korista, D. A. Verner, J. W. Ferguson, J. B. Kingdon, and E. M. Verner, Publ. Astron. Soc. Pac. **110**, 761 (1998).
[8] T. R. Kallman and M. Bautista, Astrophys. J., Suppl. Ser. **133**, 221 (2001).
[9] K. T. Borkowski, W. J. Lyerly, and S. P. Reynolds, Astrophys. J. **548**, 820 (2001).
[10] J. S. Kaastra and R. Mewe, Astron. Astrophys. Suppl. Ser. **97**, 443 (1993).
[11] R. D. Cowan, *The Theory of Atomic Structure and Spectra* (University of California Press, Berkeley, 1981).
[12] N. R. Badnell, J. Phys. B **19**, 3827 (1986).
[13] N. R. Badnell, J. Phys. B **30**, 1 (1997).
[14] H. A. Bethe and E. E. Salpeter, *Quantum Mechanics of One- and Two-Electron Atoms* (Academic, New York, 1957).
[15] W. Eissner, M. Jones, and H. Nussbaumer, Comput. Phys. Commun. **8**, 257 (1974).
[16] P. Palmeri, C. Mendoza, T. R. Kallman, and M. A. Bautista, Astron. Astrophys. **403**, 1175 (2003).
[17] M. H. Chen, K. J. Reed, D. M. McWilliams, D. S. Guo, L. Barlow, M. Lee, and V. Walker, At. Data Nucl. Data Tables **65**, 289 (1997).
[18] I. P. Grant, B. J. McKenzie, P. H. Norrington, D. F. Mayers, and N. C. Pyper, Comput. Phys. Commun. **21**, 207 (1980).
[19] M. H. Chen, Phys. Rev. A **31**, 1449 (1985).
[20] T. W. Gorczyca, C. N. Kodituwakku, K. T. Korista, O. Zatsarinny, N. R. Badnell, E. Behar, M. H. Chen, and D. W. Savin, Astrophys. J. **592**, 636 (2003).
[21] T. W. Gorczyca, I. Dumitriu, M. F. Hasoğlu, K. T. Korista, N. R. Badnell, D. W. Savin, and S. T. Manson, Astrophys. J. Lett. **638**, L121 (2006).
[22] M. F. Hasoğlu, T. W. Gorczyca, K. T. Korista, S. T. Manson, N. R. Badnell, and D. W. Savin, Astrophys. J. Lett. **649**, L149 (2006).
[23] D. W. Savin, S. M. Kahn, G. Gwinner, M. Grieser, R. Repnow, G. Saathoff, D. Schwalm, A. Wolf, A. Müller, S. Schippers, P. A. Zavodszky, M. H. Chen, T. W. Gorczyca, O. Zatsarinny, and M. F. Gu, Astrophys. J., Suppl. Ser. **147**, 421 (2003).
[24] D. W. Savin, S. M. Kahn, A. Linkeman, A. A. Saghiri, M. Schmitt, M. Grieser, R. Repnow, D. Schwalm, A. Wolf, T. Bartsch, A. Müller, S. Schippers, M. H. Chen, N. R. Badnell, T. W. Gorczyca, and O. Zatsarinny, Astrophys. J. **576**, 1098 (2002).
[25] D. W. Savin, E. Behar, S. M. Kahn, G. Gwinner, A. A. Saghiri, M. Schmitt, M. Grieser, R. Repnow, D. Schwalm, A. Wolf, T. Bartsch, A. Müller, S. Schippers, M. H. Chen, N. R. Badnell, and T. W. Gorczyca, Astrophys. J., Suppl. Ser. **138**, 337 (2002).
[26] I. P. Grant, J. Phys. B **7**, 1458 (1974).
[27] J. Von Neumann and E. Wigner, Phys. Z. **30**, 465 (1929).
[28] B. H. Bransden and C. J. Joachain, *Physics of Atoms and Molecules* (Prentice Hall, New York, 2002), Sec. 10.3.
[29] See also C. Cohen-Tannoudji, B. Diu, and F. Laloë, *Quantum Mechanics* (Wiley, New York, 2005), Section IV C; Ref. [11], Section 10-7; H. Friedrich, *Theoretical Atomic Physics* (Springer-Verlag, Berlin, 1998), Problem 1.5.
[30] A. A. Wills, T. W. Gorczyca, N. Berrah, B. Langer, Z. Felfli, E. Kukk, J. D. Bozek, O. Nayandin, and M. Alshehri, Phys. Rev. Lett. **80**, 5085 (1998).
[31] T. W. Gorczyca, Z. Felfli, H.-L. Zhou, and S. T. Manson, Phys. Rev. A **58**, 3661 (1998).
[32] M. C. Witthoeft, A. D. Whiteford, and N. R. Badnell, J. Phys. B **40**, 2969 (2007).